Electronic Supplementary Information

Hierarchical MoS_2@MoP Core-Shell Heterojunctions Electrocatalysts for Efficient Hydrogen Evolution Reaction over a Broad pH Range

Aiping Wu[a], Chungui Tian[b], Haijing Yan[b], Yanqing Jiao[b], Qing Yan[b], Guoyu Yang[a*] and Honggang Fu[b*]

[a] Key Laboratory of Cluster Science, Ministry of Education of China, Beijing Institute of Technology, Beijing 100081, China

[b] Key Laboratory of Functional Inorganic Material Chemistry, Ministry of Education of the People's Republic of China, Heilongjiang University, Harbin 150080

E-mail: ygy@bit.edu.cn, fuhg@vip.sina.com

The content of ESI

1. Figure S1. The low-magnification TEM and HRTEM images of HF-MoSP-800 (Figure S1a and b) and HF-MoSP-900 (Figure S1c and d).

2. Figure S2. SEM images of HF-MoSP-700 (a) and MoSP-1000 (b)

3. Figure S3. XRD patterns of HF-MoS_2, HF-MoSP-700, HF-MoSP-800, HF-MoSP-900 and MoSP-1000.

4. Figure S4. (a) XPS survey spectra of HF-MoS_2, HF-MoSP-700 and MoSP-1000; High resolution XPS spectra of (b) Mo 3d and (c) S 2p for HF-MoS2 samples; High resolution XPS spectra of (d) Mo 3d and (e) S 2p and (f) P 2p for HF-MoSP-700 samples; High resolution XPS spectra of (g) Mo 3d and (h) S 2p and (i) P 2p for MoSP-1000 samples.

5. Figure S5. The work function (WF) drawings of MoSP-1000.

6. Figure S6. Nitrogen adsorption–desorption isotherm of HF-MoSP-700, HF-MoSP-800, HF-MoSP-900 and HF-1000 samples.

7. Figure S7. Polarization curves for HF-MoSP-700 in (a) 0.5 M H_2SO_4 and (c) 1M KOH with a scan rate of 5 mV s^{-1}. Tafel plots for HF-MoSP-700 in (b) 0.5 M H_2SO_4 and (d) 1M KOH.

8. Figure S8. Tafel plots for HF-MoS_2, HF-MoSP-800, HF-MoSP-900 and MoSP-1000 and Pt/C

9. Figure S9. CVs for different samples with different rates from 20 to 200 mV s^{-1}.

The inset is the capacitive current at 0.15 V as a function of scan rate ($\Delta j_0 = j_a - j_c$).

10. Figure S10. Polarization curves for HF-MoSP-800 and HF-MoSP-900 at different pH: (a) pH=4.11 (weak acid condition), (b) pH=7 (neutral conditions) and (c) pH= 10.16 (weak alkaline conditions).

11. Table S1. The performance summary of different catalyst in 0.5M H_2SO_4.

12. Table S2. Comparison of HER performance of HF-MoSP with other non-noble metal HER electrocatalysts in acid and alkaline conditions

13. Table S3. The performance summary of different catalyst in 1M KOH.

1**4.** Table S4. The performance summary of HF-MoSP-800 and HF-MoSP-900 at different pH conditions

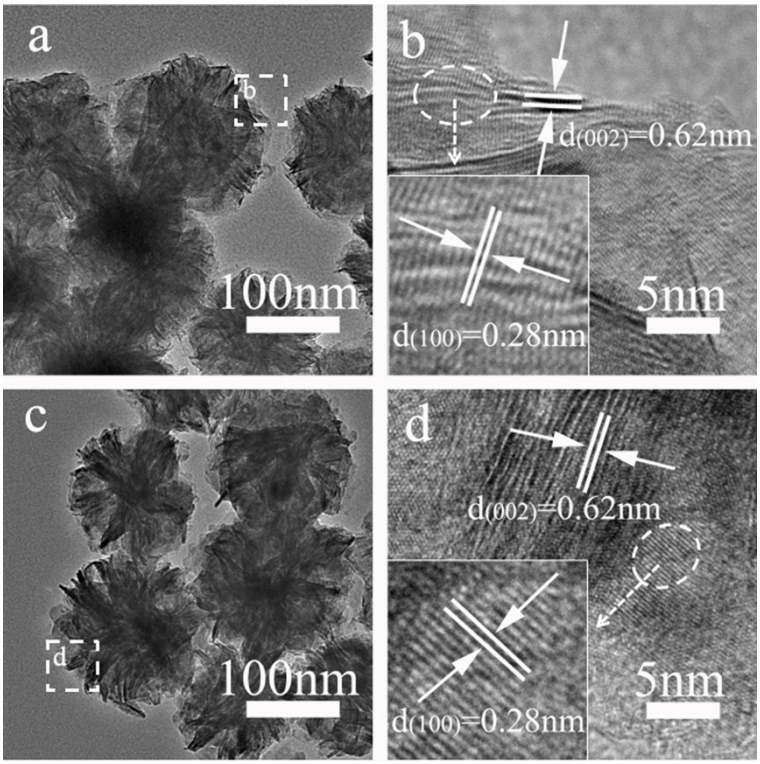

Figure S1. The low-magnification TEM and HRTEM images of HF-MoSP-800 (Figure S1a and b) and HF-MoSP-900 (Figure S1c and d).

Figure S1 shows the low-magnification TEM and HRTEM images of HF-MoSP-800 (Figure S1a and b) and HF-MoSP-900 (Figure S1c and d). The sphere-like structure have no large change before and after phosphorization reaction. The HRTEM test shows the formation of the thin sheet-like structure on outside surface of HF-MoSP-800, instead of the silk ribbon-liked structure in original HF-MoS_2 samples (Figure 1d). The presence of intimately contacted MoS_2 and MoP phase can be verified by HRTEM. The plane distance of 0.62 nm (002 for MoS_2) and 0.28 nm (100 for MoP) can be obviously seen (Figure S1c). The plane distance of 0.62 nm (002 for MoS_2) and 0.28 nm (100 for MoP) can be obviously seen (Figure S1d).

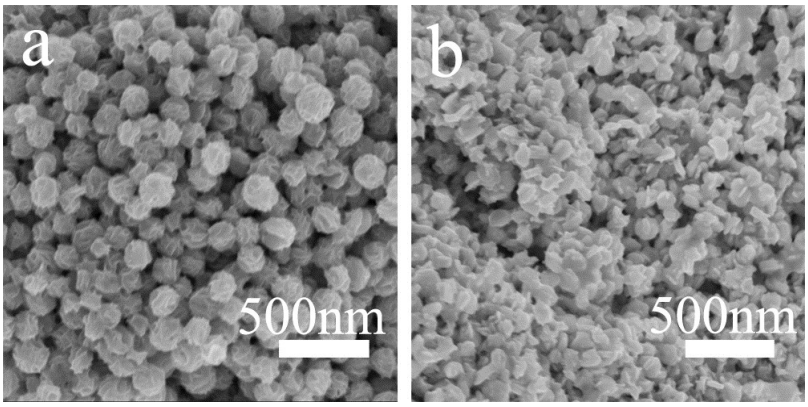

Figure S2. SEM images of HF-MoSP-700 (a) and MoSP-1000 (b)

Figure S2 shows SEM images of HF-MoSP-700 (a) and MoSP-1000 (b). We can see that the hierarchical spherical structure can be well remained for HF-MoSP-700 samples. The size and surface morphology have no obvious change after the phosphorization at 700 ^{o}C. However, for MoSP-1000 sample, a lager change can happened. The low-magnification SEM image in Figure S2b shows the presence of irregular particles with size smaller than that of HF-MoS_2 sample. The irregular shape and smaller size should be due to destroying and shrink of HF-MoS_2.

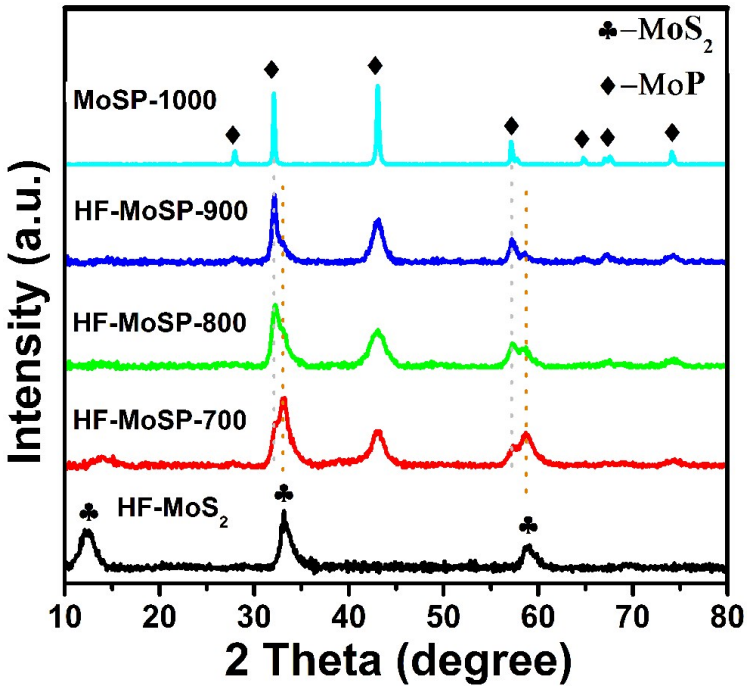

Figure S3. XRD patterns of HF-MoS_2, HF-MoSP-700, HF-MoSP-800, HF-MoSP-900 and MoSP-1000.

XRD patterns of different sample are shown in Figure S3. For HF-MoS_2, the intensive peaks about MoS_2 can be seen. The peaks located at about 13°, 33° and 59° can be indexed to the (002), (100) and (110) diffraction of hexagonal structured MoS_2. After the phosphorization at 700 °C, the 2 θ value of (002) diffraction peak was shifted to 14° revealing the decreased interlayer distance of (002) plane from 0.7 to 0.62nm and the new peaks at 32 °, 43° and 57° emerge, corresponding to the diffraction of (100), (101) and (110) of MoP, respectively (JCPDS No. 89–5110), besides the peaks belonging to MoS_2. The results indicate that the samples are composed of MoP and MoS_2 composite. The peak intensity of MoP phase increases gradually with the increase of phosphorization temperature. The intensity ratios of (100) diffraction of MoP/MoS_2 phase are about 0.63, 1.7 and 2.6 for HF-MoSP-700, HF-MoSP-800 and HF-MoSP-900 samples. For MoSP-1000 sample, the intensive peaks belonging to MoP phase can be seen, and those corresponding to MoS_2 are not obvious. The results show that the microstructure (phosphorization degree) can be well tuned. Also, we can see that the hierarchical structure can be well remained at broad temperature range until the 900°C. The stability of the hierarchical, spherical

structures at broad range provides large space for the preparation of hierarchical MoSP with tuned structure, being favourable for tuning the performance of the materials.

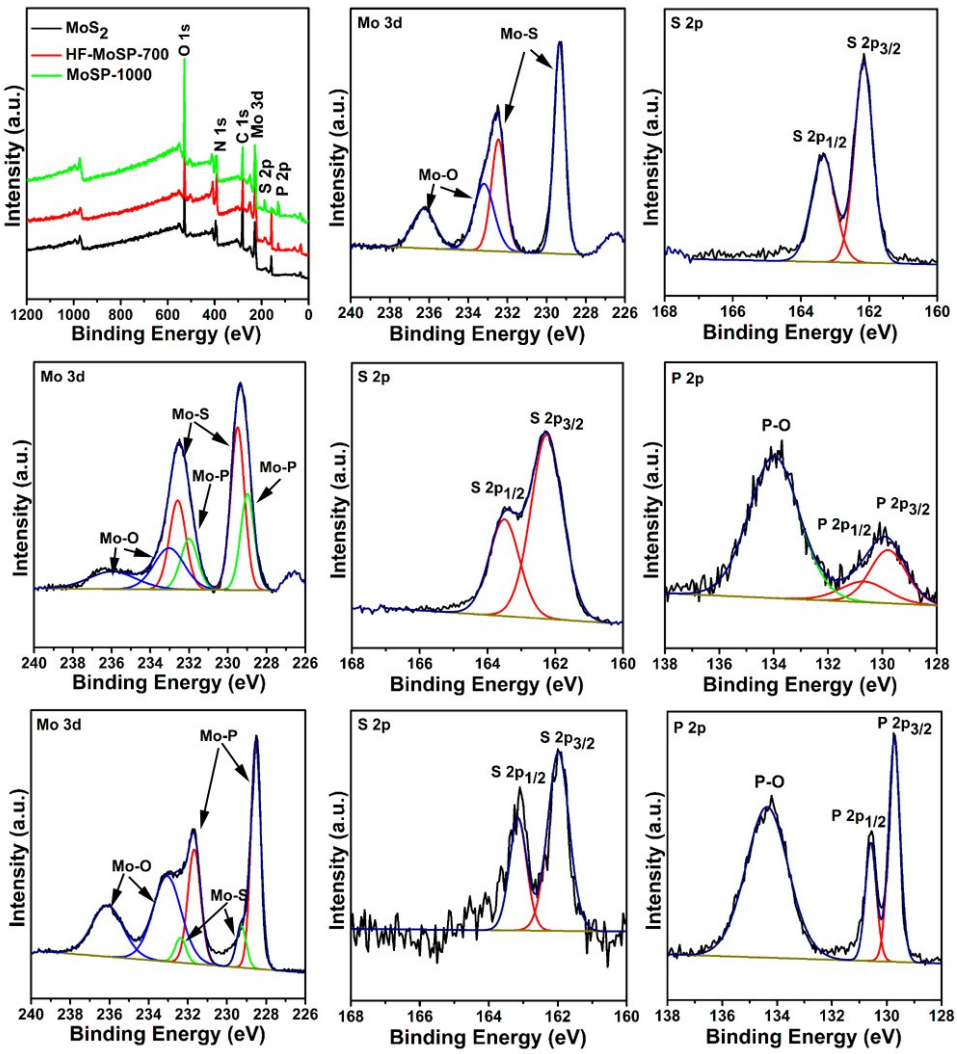

Figure S4. (a) XPS survey spectra of HF-MoS_2, HF-MoSP-700 and MoSP-1000; High resolution XPS spectra of (b) Mo 3d and (c) S 2p for HF-MoS_2 samples; High resolution XPS spectra of (d) Mo 3d and (e) S 2p and (f) P 2p for HF-MoSP-700 samples; High resolution XPS spectra of (g) Mo 3d and (h) S 2p and (i) P 2p for MoSP-1000 samples.

Figure S4a shows the XPS survey spectra of HF-MoS_2, HF-MoSP-700 and

MoSP-1000 samples. The XPS spectrum (Figure S4a) shows the presence of Mo, S elements and no P sign is observed. For the samples from phosphorization (HF-MoSP-700 and MoSP-1000), the obvious sign of P 2p can be detected. The Mo 3d spectra of all samples show the peaks corresponding to Mo-S (232.45 and 229.4eV) and Mo-O (233.1 eV and 236.05 eV). The appearance of Mo-O should due to the slight surface oxidation of samples after the exposure to air. For all samples, the S $2p_{1/2}$ and $2p_{3/2}$ of S 2p are located at 163.45 and 162.2 eV, which can be ascribed to the S^{2-} from MoS_2. For HF-MoSP-700 and MoSP-1000, the doublet peaks at about 129.55 eV and 130.4 eV can be indexed to P bonded to Mo in the form of a MoP. The P/S atom ratio is about 0.12, 0.24, 0.53 and 1.96 for HF-MoSP-700, HF-MoSP-800, HF-MoSP-900 and MoSP-1000, indicating an enhancement of MoP content with the increase of temperature. For HF-MoS_2, there are no detectable P sign. For MoSP-1000, only very low content of S can be observed. The results further indicate that the phosphorization degree can be well tuned just by tuning the phosphorization temperature.

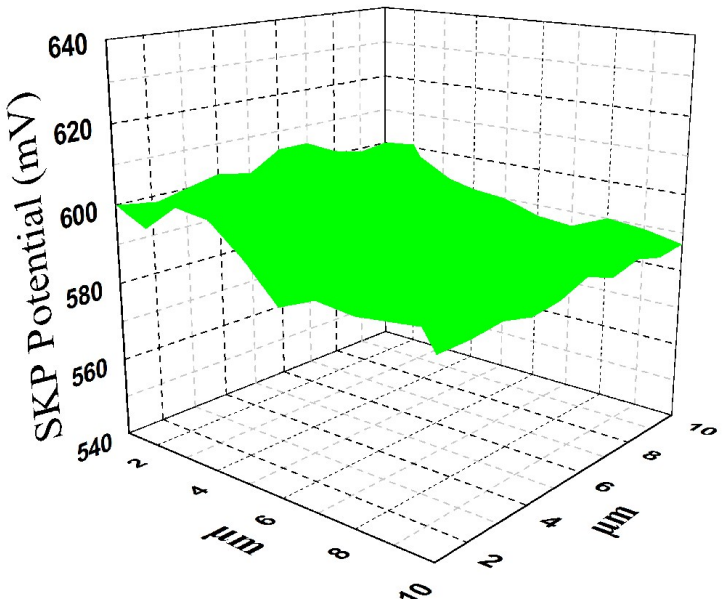

Figure S5. The work function (WF) drawings of MoSP-1000.

Figure S5 shows the work function drawings of MoSP-1000 samples. The work function value of MoSP-1000 is 5.93 eV, which is larger than other samples. Although the higher WF of MoSP-1000 than HF-MoSP-800 and HF-MoSP-900, the MoSP-1000 shows the poor performance for HER than HF-MoSP-800 and HF-MoSP-900, which should be ascribed to the low SBET of MoSP-1000.

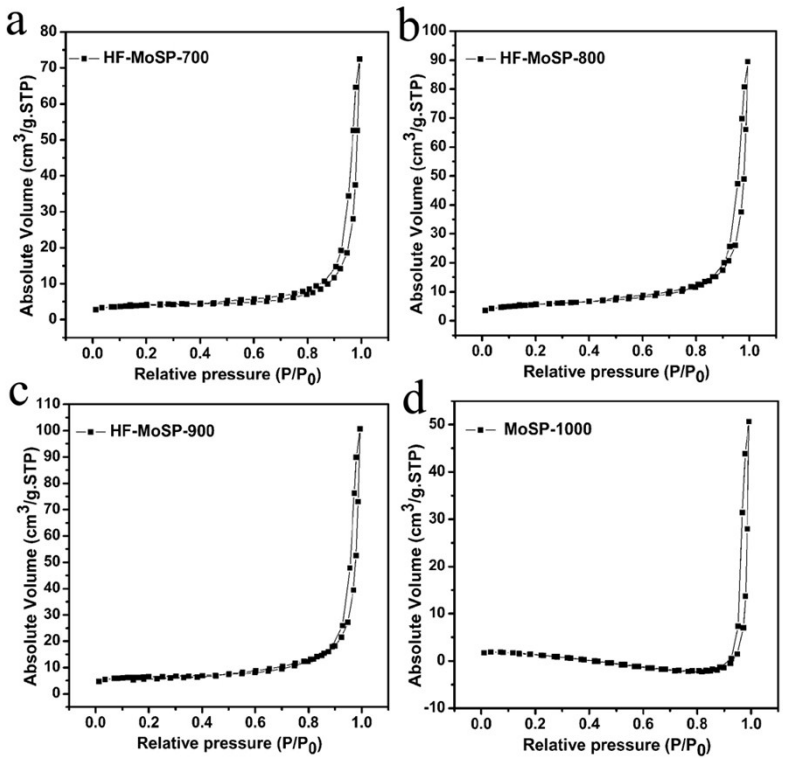

Figure S6. Nitrogen adsorption–desorption isotherm of HF-MoSP-700, HF-MoSP-800, HF-MoSP-900 and MoSP-1000 samples.

The BET specific area of HF-MoSP-700, HF-MoSP-800, HF-MoSP-900 and MoSP-1000 are about 13.9, 19.7, 22.1 and 4.0 m^2 g^{-1}. The small value of MoSP-1000 implies the destroying the hierarchical structure, being consistent with TEM and SEM observation.

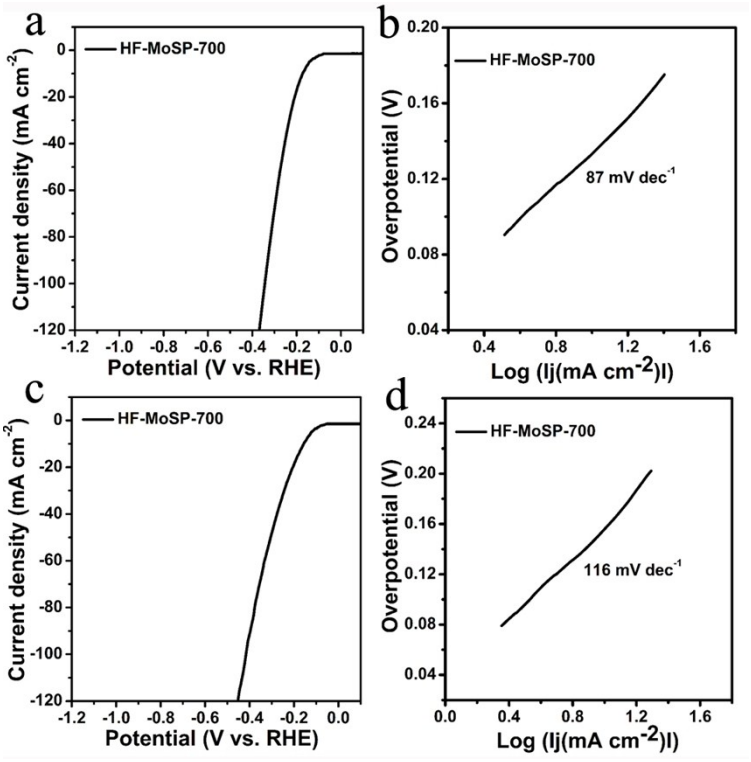

Figure S7. Polarization curves for HF-MoSP-700 in (a) 0.5 M H_2SO_4 and (c) 1M KOH with a scan rate of 5 mV s^{-1}. Tafel plots for HF-MoS-700 in (b) 0.5 M H_2SO_4 and (d) 1M KOH.

Figure S7 shows the polarization curves and onset potentials for HF-MoSP-700 in 0.5 M H_2SO_4 and 1M KOH. The onset potential are about (a) 89 mV in 0.5 M H_2SO_4 and (c) 76 mV in 1M KOH. Tafel plots for HF-MoSP-700 in (b) 0.5 M H_2SO_4 and (d) 1M KOH are about 87mV dec^{-1} and 116mV dec^{-1}, respectively.

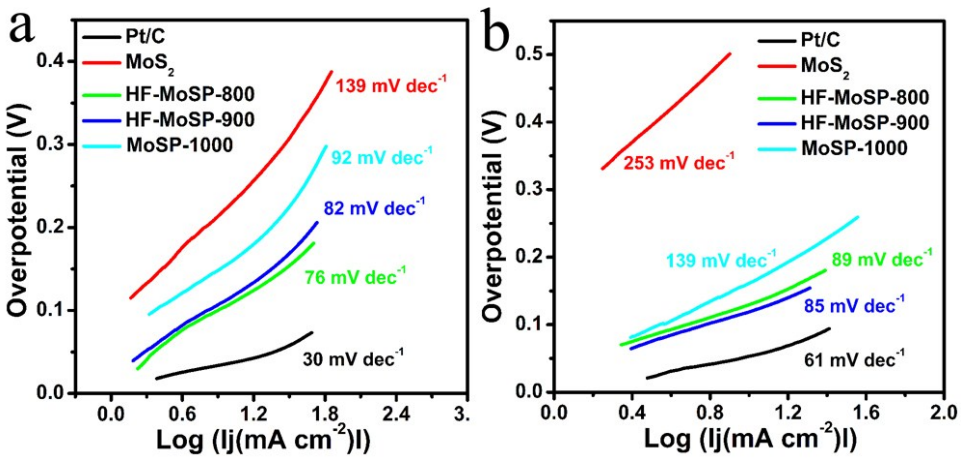

Figure S8. Tafel plots for HF-MoS_2, HF-MoSP-800, HF-MoSP-900 and MoSP-1000 and Pt/C.

The Tafel plots are fitted to the Tafel equation ($\eta=b\log j+a$, where j is the current density and b is the Tafel slope). The Tafel slopes of approximately 30, 139, 76, 82 and 92mVdec^{-1} for Pt/C, HF-MoS_2, HF-MoSP-800, HF-MoSP-900 and MoSP-1000 in 0.5M H_2SO_4 (Figure S8a), respectively. In 1M KOH, the Tafel slopes is about 61, 253, 89, 85 and 139 mV dec-1 for Pt/C, HF-MoS_2, HF-MoSP-800, HF-MoSP-900 and MoSP-1000 (Figure S8b), respectively.

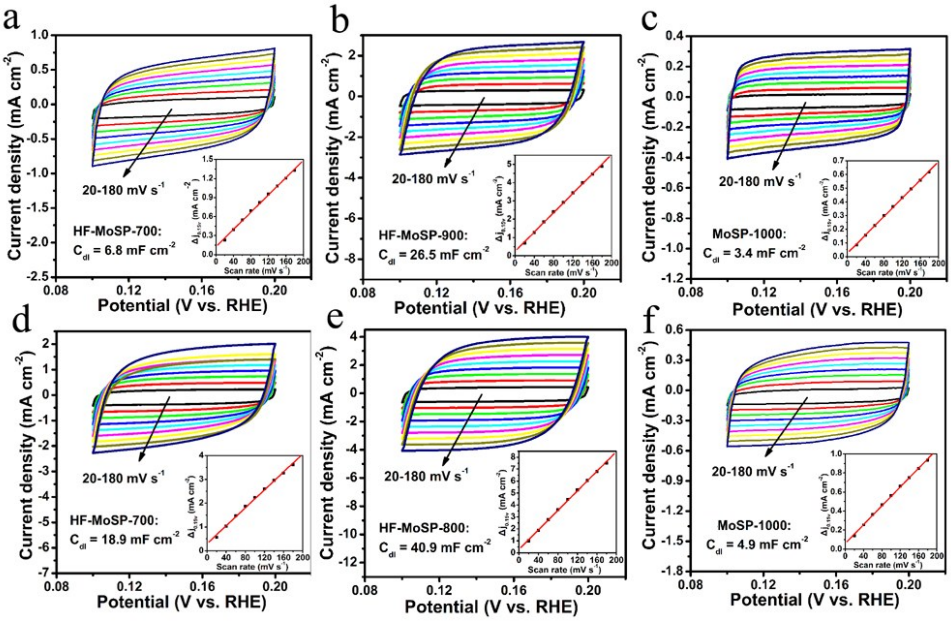

Figure S9. CVs for different samples with different rates from 20 to 180 mV s^{-1}. The inset is the capacitive current at 0.15 V as a function of scan rate ($\Delta j_0 = j_a - j_c$).

The capacitance is 6.8 mF cm^{-2} (Figure S9a), 41.6 mF cm^{-2} (Figure 6b), 26.5 mF cm^{-2} (Figure S9b) and 3.4 mF cm^{-2} (Figure S9c) in 0.5 M H_2SO_4 for HF-MoSP-700, HF-MoSP-800, HF-MoSP-900 and MoSP-1000 samples.

In 1M KOH, the capacitance is 18.9 mF cm^{-2} (Figure S9d), 40.9 mF cm^{-2} (Figure S9e), 45.3 mF cm^{-2} (Figure 6e) and 4.9 mF cm^{-2} (Figure S9f) for HF-MoSP-700, HF-MoSP-800, HF-MoSP-900 and MoSP-1000 samples.

We can see that the HF-MoSP-800 shows the highest capacitance in 0.5M H_2SO_4, and HF-MoSP-900 gives the highest capacitance in 1M KOH, which should be responsible for the good performance of HF-MoSP-800 and HF-MoSP-900 in 0.5M H_2SO_4 and in 1M KOH.

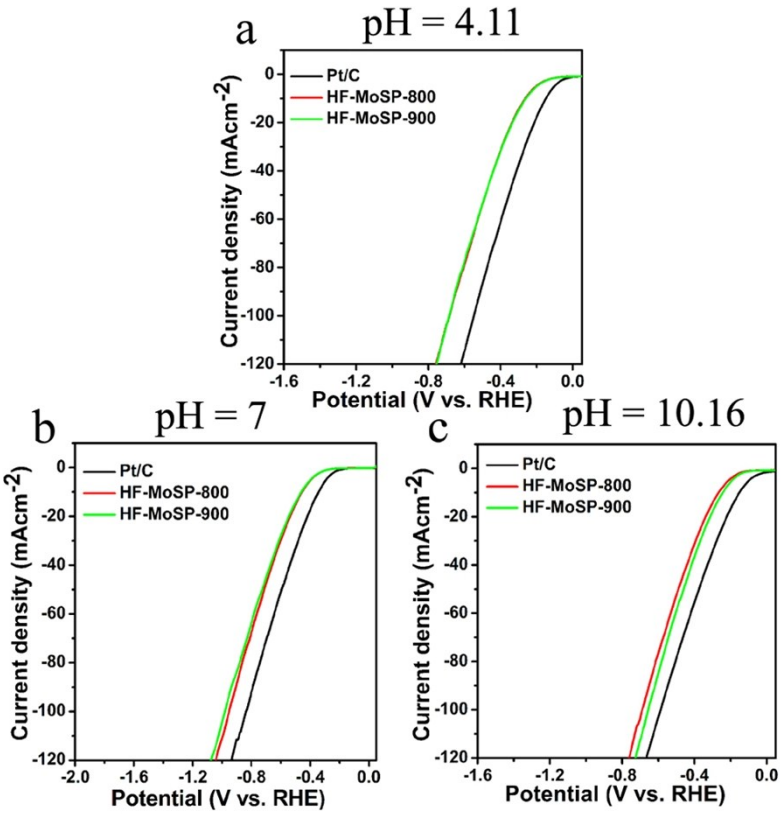

Figure S10. Polarization curves for HF-MoSP-800 and HF-MoSP-900 at different pH: (a) pH=4.11 (weak acid condition), (b) pH=7 (natural conditions) and (c) pH= 10.16 (weak alkaline conditions).

Figure S10 shows the polarization curves for HF-MoSP-800 and HF-MoSP-900 at pH=4.11 (weak acid condition), (b) pH=7 (natural conditions) and (c) pH=10.16 (weak alkaline conditions). The onset potential and η at 10 mA cm^{-2} are listed at Table S1. We can seen that the samples show the obvious catalytic activity for HER under different pH conditions. By combination of the test at pH=0 and pH=14, we can say that the HF-MoSP catalyst is promising catalyst for HER in all pH range.

Table S1. The performance summary of different catalyst at pH=0 (0.5M H_2SO_4)

Samples	**HF-MoS_2**	**HF-MoSP-700**	**HF-MoSP-800**	**HF-MoSP-900**	**MoSP-1000**
Onset potential (mV)	**121**	**89**	**29**	**40**	**68**
η (mV) at 10mAcm^{-2}	**228**	**164**	**108**	**116**	**158**
Tafel slope (mV/dec)	**139**	**87**	**76**	**82**	**92**

Table S2. Comparison of HER performance of HF-MoSP with other non-noble metal HER electrocatalysts in acid and alkaline condition

Catalyst	Catalyst amount (mg cm^{-2})	Onset potential (mV)	Overpotential at 10 mA cm^{-2}	Electrolyte solution	Ref.
HF-MoSP	0.35	29	108	0.5 M H_2SO_4	**This**
		40	116	1 M KOH	**work**
metallic MoS_2 nanosheets	-	150	187	0.5 M H_2SO_4	**1**
MoS_2 nanosheets	0.285	100	~180	0.5 M H_2SO_4	**2**
defect-rich MoS_2	0.285	120	~190	0.5 M H_2SO_4	**3**
MoS_2@OMC	0.3	120	178	0.5 M H_2SO_4	**4**
MoP-CA2	0.36	40	125	0.5 M H_2SO_4	**5**
MoP	0.86	50	130	0.5 M H_2SO_4	**6**
		55	140	1 M KOH	
MoP/Ti	1	-	110	0.5 M H_2SO_4	**7**
MoP/FTO	0.1	80	150	0.5 M H_2SO_4	**8**
		~95	190	1 M KOH	
MoP	0.071	100	246	0.5 M H_2SO_4	**9**
MoP|S-CB	0.3	70	150	0.5 M H_2SO_4	**10**
MoP| S-Ti	3	20	64	0.5 M H_2SO_4	**11**
$MoS_{2(1-x)}P_x$	0.285	-	120	0.5 M H_2SO_4	**12**
Mo_2C nanotubes	0.8	82	172	0.5 M H_2SO_4	**13**
		37	112	0.1 M KOH	
MoCx nano-octahedrons	0.8	25	142	0.5 M H_2SO_4	**14**
		80	151	1 M KOH	
MoDCA-5	0.25	6	78	0.5 M H_2SO_4	**15**
Mo_2C@NC	0.28	< 60	124	0.5 M H_2SO_4	**16**
		-	60	1 M KOH	
Mo_xC-Ni@NCV	1.1	-	68	0.5 M H_2SO_4	**17**
		-	126	1 M KOH	
MoB	2.5	> 100	~215	0.5 M H_2SO_4	**18**
		140	225	1 M KOH	
CoP/CC	0.92	38	67	0.5 M H_2SO_4	**19**
		80	209	1 M KOH	
CoP/CNT	0.285	40	122	0.5 M H_2SO_4	**20**
Ni_5P_4 on	-	-	140	0.5 M H_2SO_4	**21**
Nickel foil		-	150	1 M KOH	
Cu_3P NWs/CF	15.2	62	143	0.5 M H_2SO_4	**22**
Co-NRCNTs	0.28	50	260	0.5 M H_2SO_4	**23**
			370	1 M KOH	
NiO/Ni-CNT	0.28	-	80	1 M KOH	**24**
C_3N_4 @NG	0.1	~150	~240	0.5 M H_2SO_4	**25**
		-	> 600	1 M KOH	
Ni/NiO-NSA	-	34	~110	0.1M KOH	**26**

From Table S2, we can see that the HF-MoSP give good activity under both acid (pH=0) and alkaline (pH=14) conditions. It has shown enhanced comprehensive performance in comparison with Mo-based catalysts, such as MoS_2, MoP and MoC (Ref. 1, 2, 3, 4, 5, 6, 8, 9, 10, 12, 13, 14), and phosphide (CoP/CNT, Ni_5P_4 and Cu_3P NWs/CF) (Ref. 20, 21 and 22).

The catalytic performance of catalyst can also be affected by the catalyst loading. A high loading would be favorable to improve the performance of the catalysts. We think that the performance of HF-MoSP can be further improved by growth of them on suitable supports with high loading such as carbon cloth and Ti plate etc.

Table S3. The performance summary of different catalyst at pH=14 (1M KOH)

Samples	**HF-MoS_2**	**HF-MoSP-700**	**HF-MoSP-800**	**HF-MoSP-900**	**MoSP-1000**
Onset potential (mV)	**227**	**76**	**50**	**42**	**69**
η (mV) at 10mAcm^{-2}	**530**	**156**	**128**	**119**	**161**
Tafel slope (mV/dec)	**258**	**116**	**89**	**85**	**139**

Table S4. The performance summary of HF-MoSP-800 and HF-MoSP-900 at different pH conditions

pH=4.11

Samples	HF-MoSP-800	HF-MoSP-900
Onset potential (mV)	55	48
η (mV) at 10mAcm^{-2}	263	261

pH=7

Samples	HF-MoSP-800	HF-MoSP-900
Onset potential (mV)	233	242
η (mV) at 10mAcm^{-2}	456	460

pH=10.16

Samples	HF-MoSP-800	HF-MoSP-900
Onset potential (mV)	85	72
η (mV) at 10mAcm^{-2}	266	244

Reference List:

[1] M. A. Lukowski, A. S. Daniel, F. Meng, A. Forticaux, L. Li and S. Jin, J. Am. Chem. Soc. **2013**, 135, 10274 - 10277.
[2] J. Xie, J. Zhang, S. Li, F. Grote, X. Zhang, H. Zhang, R. Wang, Y. Lei, B. Pan and Y. Xie, J. Am. Chem. Soc. **2013**, 135, 17881 - 17888.
[3] J. Xie, H. Zhang, S. Li, R. Wang, X. Sun, M. Zhou, J. Zhou, X. Lou and Y. Xie, Adv. Mater. **2013**, 25, 5807 - 5813.
[4] B. Seo, G. Y. Jung, Y. J. Sa, H. Y. Jeong, J. Y. Cheon, J. H. Lee, H. Y. Kim, J. C. Kim, H. S. Shin, S. K. Kwak and S. H. Joo, ACS Nano **2015**, 9, 3728 - 3739.
[5] Z. C. Xing, Q. Liu, A. M. Asiri and X. P. Sun, Adv. Mater. **2014**, 26, 5702 - 5707.
[6] P. Xiao, M. A. Sk, L. Thia, X. Ge, R. J. Lim, J. Y. Wang, K. H. Lim and X. Wang, Energy Environ. Sci. **2014**, 7, 2624 - 2629.
[7] J. M. McEnaney, J. C. Crompton, J. F. Callejas, E. J. Popczun, A. J. Biacchi, N. S. Lewis and R. E. Schaak, Chem. Mater. **2014**, 26, 4826 - 4831.
[8] T. Y. Wang, K. Z. Du, W. L. Liu, Z. W. Zhu, Y. H. Shao and M. X. Li, J. Mater. Chem. A **2015**, 3, 4368 - 4373.
[9] X. B. Chen, D. Z. Wang, Z. P. Wang, P. Zhou, Z. Z. Wu and F. Jiang, Chem. Commun. **2014**, 50, 11683 - 11685.
[10] J. W. Desmond Ng, T. R. Hellstern, J. Kibsgaard, A. C. Hinckley, J. D. Benck

and T. F. Jaramillo, ChemSusChem **2015**, 8, 3512 - 3519.
[11] J. Kibsgaard and T. F. Jaramillo, Angew. Chem. Int. Ed. **2014**, 126, 14661 - 14665.
[12] R. Q. Ye, P. D. Angel-Vicente, Y. Y. Liu, M. J. Arellano-Jimenez, Z. W. Peng, T. Wang, Y. L. Li, B. I. Yakobson, S. H. Wei, M. J. Yacaman and J. M. Tour, Adv. Mater. **2015**, DOI:10.1002/adma.201504866.
[13] F. X. Ma, H. B. Wu, B. Y. Xia, C. Y. Xu and X. W. Lou, Angew. Chem. Int. Ed. **2015**, 54, 15395-15399.
[14] H. B. Wu, B. Y. Xia, L. Yu, X. Y. Yu and X. W. Lou, Nat. Commun. **2015**, 6, DOI: 10.1038/ncomms7512.
[15]R. G. Ma, Y. Zhou, Y. F. Chen, P. X. Li, Q. Liu and J. C. Wang, Angew. Chem. Int. Ed. **2015**, 54, 14723 - 14727.
[16] Y. P. Liu, G. T. Yu, G. D. Li, Y. H. Sun, T. Asefa, W. Chen and X. X. Zou, Angew. Chem. Int. Ed. **2015**, 54, 10752 - 10757.
[17] S. P. Wang, J. Wang, M. L. Zhu, X. B. Bao, B. Y. Xiao, D. F. Su, H. R. Li and Y. Wang, J. Am. Chem. Soc. **2015**, 137, 15753 - 15759.
[18] H. Vrubel and X. L. Hu, Angew. Chem. Int. Ed. **2012**, 51, 12875 -12878.
[19] J. Q. Tian, Q. Liu, A. M. Asiri and X. P. Sun, J. Am. Chem. Soc. **2014**, 136, 7587 - 7590.
[20] Q. Liu, J. Q. Tian, W. Cui, P. Jiang, N. Y. Cheng, A. M. Asiri and X. P. Sun, Angew. Chem. Int. Ed. **2014**, 126, 6828 - 6832.
[21] M. Ledendecker, S. K. Caldern, C. Papp, H. P. Steinrck, M. Antonietti and M. Shalom, Angew. Chem. Int. Ed. **2015**, 127, 12538 - 12542.
[22] J. Q. Tian, Q. Liu, N. Y. Cheng, A. M. Asiri and X. P. Sun, Angew. Chem. Int. Ed. **2014**, 53, 9577-9581
[23] X. X. Zou, X. X. Huang, A. Goswami, R. Silva, B. R. Sathe, E. Mikmekov and T. Asefa, Angew. Chem. Int. Ed. **2014**, 53, 4461 - 4465.
[24] M. Gong, W. Zhou, M. C. Tsai, J. G. Zhou, M. Y. Guan, M. C. Lin, B. Zhang, Y. F. Hu, D. Y. Wang, J. Yang, S. J. Pennycook, B. J. Hwang and Hongjie Dai, Nat. Commun. **2014**, 5, DOI: 10.1038/ncomms5695.
[25] Y. Zheng, Y. Jiao, Y. H. Zhu, L. H. Li, Y. Han, Y. Chen, A. J. Du, M. Jaroniec, S. Z. Qiao and Nat. Commun. **2014**, 5, DOI: 10.1038/ncomms4783.
[26] Y. Kuang, G. Feng, P. S. Li, Y. M. Bi, Y. P. Li and X. M. Sun, Angew. Chem. Int. Ed. **2016**, 55, 693 - 697.